Role of the Boundary Layer Moisture Asymmetry in Causing the Eastward Propagation of the Madden–Julian Oscillation*

PANG-CHI HSU AND TIM LI

International Pacific Research Center, and School of Ocean and Earth Science and Technology, University of Hawaii at Manoa, Honolulu, Hawaii

(Manuscript received 2 June 2011, in final form 2 February 2012)

ABSTRACT

The moisture budget associated with the eastward-propagating Madden–Julian oscillation (MJO) was diagnosed using 1979–2001 40-yr ECMWF Re-Analysis (ERA-40) data. A marked zonal asymmetry of the moisture relative to the MJO convection appears in the planetary boundary layer (PBL, below 700 hPa), creating a potentially more unstable stratification to the east of the MJO convection and favoring the eastward propagation of MJO. The PBL-integrated moisture budget diagnosis indicates that the vertical advection of moisture dominates the low-level moistening ahead of the convection. A further diagnosis indicates that the leading term in the vertical moisture advection is the advection of the background moisture by the MJO ascending flow associated with PBL convergence. The cause of the zonally asymmetric PBL convergence is further examined. It is found that heating-induced free-atmospheric wave dynamics account for 75%–90% of the total PBL convergence, while the warm SST anomaly induced by air–sea interaction contributes 10%–25% of the total PBL convergence.

The horizontal moisture advection also plays a role in contributing to the PBL moistening ahead of the MJO convection. The leading term in the moisture advection is the advection across the background moisture gradient by the MJO flow. In the western Indian Ocean, Maritime Continent, and western Pacific, the meridional moisture advection by the MJO northerly flow dominates, while in the eastern Indian Ocean the zonal moisture advection is greater. The contribution of the moisture advection by synoptic eddies is in general small; it has a negative effect over the tropical Indian Ocean and western Pacific and becomes positive in the Maritime Continent region.

1. Introduction

The Madden–Julian oscillation (MJO; Madden and Julian 1971, 1972) is the dominant mode of intraseasonal variability in the tropics. MJO is characterized by the eastward propagation of planetary-scale tropospheric circulations (Li and Zhou 2009) with a period of 30–60 days. MJO convection often initiates in the western Indian Ocean and strengthens as it propagates eastward into the eastern Indian Ocean and western Pacific (WP) (Madden and Julian 2005, Jiang and Li 2005). While passing through the eastern Pacific cold tongue, MJO tends to weaken. While observational, theoretical, and modeling studies in the past decades have advanced our understanding of MJO, some fundamental issues regarding its propagation and initiation remain open (see reviews in Zhang 2005; Waliser 2006). The limited capability in simulating and predicting MJO in state-of-art general circulation models (Lin et al. 2006; Kim et al. 2009) calls for further explorations of MJO initiation and propagation mechanisms.

Previous theoretical studies suggested that the convection–circulation feedback plays a critical role in the maintenance and propagation of MJO. On the basis of conditional instability of the second kind (CISK), the interactions between the convective heating and low-level convergence associated with equatorial Kelvin waves cause an unstable growth (Lau and Peng 1987; Chang and Lim 1988), although this unstable mode prefers a shorter zonal scale and propagates too fast ($\sim$20 m s^{-1}) compared with the observed phase speed ($\sim$5 m s^{-1}).

* School of Ocean and Earth Science and Technology Contribution Number 8565 and International Pacific Research Center Contribution Number 859.

Corresponding author address: Tim Li, IPRC, SOEST, University of Hawaii at Manoa, 1680 East West Road, POST Bldg. 401, Honolulu, HI 96822.
E-mail: timli@hawaii.edu

DOI: 10.1175/JCLI-D-11-00310.1

© 2012 American Meteorological Society

The inclusion of a planetary boundary layer (PBL) and equatorial Rossby waves slows down the eastward propagation (Wang 1988; Wang and Rui 1990). In a 2.5-layer model of Wang and Li (1994) and Li and Wang (1994), the PBL convergence appears ahead of the MJO convection as a consequence of boundary layer friction. This asymmetric zonal structure of the PBL convergence is in good agreement with the observed structure (e.g., Hendon and Salby 1994; Maloney and Hartmann 1998). While the previous studies have identified the important role of the PBL convergence asymmetry in the eastward propagation, the quantitative examination of relative roles of free-atmospheric wave dynamics, surface fluxes, and air–sea interaction induced SST changes in causing the phase leading of the PBL convergence remains absent.

Some recent studies have focused on the atmospheric moisture dynamic in relation to the MJO development and propagation (e.g., Kiladis et al. 2005; Benedict and Randall 2007; Maloney 2009, hereafter M09). An increase of lower-tropospheric moisture acts to destabilize the atmosphere prior to the arrival of MJO deep convection, and the moisture is discharged after the deep convection occurs (Bladé and Hartmann 1993; Kemball-Cook and Weare 2001; Kiladis et al. 2005). Benedict and Randall (2007) analyzed reanalysis data and found both horizontal moisture advection and moisture convergence account for the MJO moisture tendency. Based on a diagnosis of a moisture budget in an atmospheric general circulation model, M09 found that the horizontal moisture advection dominates the positive tendency of column-integrated moist statistic energy (MSE) ahead of the MJO precipitation. However, the positive MSE tendency induced by the moisture advection is to a large extent offset by the surface latent heat flux (LHF). M09 also suggested that a weakening of transient eddy activity may decrease dry advection from the extratropics, leading to the low-level moistening ahead of the MJO precipitation center.

The MSE or moisture budget analysis performed in M09 was based on the vertical integration in atmospheric column. However, as showed in section 3, the column-integrated moisture tendency primarily reflects the moisture change in the middle troposphere. In this study we will focus on the effect of the PBL moisture asymmetry because it occurs prior to the midtropospheric moistening. It will be shown that a relatively unstable stratification occurs in the PBL moistening region. In other words, the PBL moisture preconditions the subsequent development of atmospheric convection. The objective of the present study is to examine the origin of the PBL moisture asymmetry associated with MJO using the reanalysis data. We intend to clarify what are the relative roles of the surface fluxes, PBL convergence, and moisture advection in contributing to the observed moisture asymmetry. Whether or not the synoptic-scale eddy plays a role in affecting the PBL moisture asymmetry will also be examined.

The rest of the paper is organized as follows. Section 2 describes the data and methodology. Section 3 presents the diagnosis results of the moisture budgets in the eastern Indian Ocean where the MJO is in a peak phase. Section 4 discusses the roles of free-atmospheric wave dynamic and the wind–evaporation–SST feedback in causing the PBL convergence ahead of MJO convection. Section 5 compares the MJO moisture budget results in different locations over the western Indian Ocean, Maritime Continent (MC), and western Pacific. Finally, a summary and discussions are given in section 6.

2. Data and methods

a. Data

The reliability of a moisture budget analysis depends crucially on the quality of reanalysis data used. The structure of intraseasonal moisture profile based on the 40-yr European Centre for Medium-Range Weather Forecasts (ECMWF) Re-Analysis (ERA-40) (Uppala et al. 2005) is consistent with the radiosonde data and remotely sensed vapor measurement (Benedict and Randall 2007). A comparison of intraseasonal apparent heating fields calculated based on the ERA-40 and observational radiosonde data over the South China Sea also shows that this reanalysis dataset captures well the amplitude and evolution of the heating fields (Hsu and Li 2011). Thus daily-averaged ERA-40 is adopted for the moisture diagnosis in this study. The ERA-40 three-dimensional (3D) atmospheric reanalysis product contains zonal and meridional wind (u and v) components, vertical p velocity (ω), and geopotential (ϕ) and specific humidity (q) fields at 17 levels from 1000 to 100 hPa. The dataset is used to diagnose the moisture budget and describe 3D dynamic and thermodynamic structures of MJO. The surface products of ERA-40 include evaporation, 10-m wind, sea surface specific humidity, and 2-m temperature, the last three of which are used to compute the surface latent heat flux based on a bulk formula (Weare et al. 1981). For the current analysis, we focus on the MJO evolution during northern winter months from December to February (DJF). The ERA-40 dataset is defined at a $2.5° \times 2.5°$ latitude–longitude grid, extending for a period from 1979 to 2001.

Other datasets used in this study include (i) observed daily outgoing longwave radiation (OLR) from the National Oceanic and Atmospheric Administration (NOAA)

polar-orbiting satellites (Liebmann and Smith 1996), (ii) daily SST from version 2 National Oceanic and Atmospheric Administration Optimal Interpolation (NOAA OI) based upon Advanced Very High Resolution Radiometer (AVHRR) satellite (Reynolds et al. 2002), and (iii) daily evaporation from the Objectively Analyzed Air–Sea Fluxes (OAFlux) (Yu and Weller 2007). The observed OLR is used to represent MJO deep convection. It covers a period of 1979–2001 and has a resolution of 2.5° × 2.5°. To unify the spatial resolutions among datasets, the higher-resolution NOAA OI SST (0.25° grid point) and OAFlux evaporation (1° grid point) are averaged and transformed into a global 2.5° grid. The SST data cover the period from 1981 to 2001, while the OAFlux is from 1985 to 2001.

b. Filtering and MJO phase definition

Since the MJO has distinct spatial and temporal characteristics from other convectively coupled tropical wave (Wheeler and Kiladis 1999), a wavenumber–frequency filtering method similar to Kiladis et al. (2005) and Benedict and Randall (2007) is used to extract the eastward-propagating MJO signal. As a result of this spatial–temporal filtering, only zonal wavenumber 1–5 and period of 20–80 days are retained. To examine the contribution to the MJO moisture budget by other time scale motions, a 10-day high-pass filter and a 90-day low-pass filter are applied to extract the synoptic-scale disturbances and the low-frequency background state (LFBS) signals from the raw data, respectively.

Figure 1 shows that the maximum variances of MJO-filtered OLR and 850-hPa zonal wind fields both appear in the southern equatorial regions of the Indian and Pacific Oceans during boreal winter. The maximum MJO convective activity and circulation centers coincide with the maximum seasonal mean precipitation zone, suggesting the large-scale control of the mean circulation on MJO. Since the LFBS flow exhibits different characteristics over the tropical Indian and Pacific Oceans, interactions among the LFBS flow, MJO and synoptic eddy may vary geographically. Taking the longitudinal dependence of MJO-related moisture dynamics into account, four equally spaced MJO convection centers (each of which has a 10° × 10° box area) are selected along the maximum MJO activity zone. They represent MJO activity over the western Indian Ocean (WIO; 5°–15°S, 60°–70°E), eastern Indian Ocean (EIO; 0°–10°S, 90°–100°E), MC (5°–15°S, 120°–130°E), and WP (5°–15°S, 150°–160°E), respectively. The detailed diagnoses of MJO structure and moisture budget will be conducted in the WIO, EIO, MC, and WP.

The MJO active and suppressed phases are defined when the MJO-filtered OLR time series at each box exceeds negative and positive one standard deviation. Based on this criterion, 233, 240, 270, and 253 cases are selected from the WIO, EIO, MC, and WP regions for the MJO active phase composites, and 236, 292, 248, and 186 cases are selected for the MJO suppressed phase composites. Because the composite results for the MJO active and suppressed phases are quite similar (with an opposite sign), only the MJO active phase composites are shown in this paper.

c. Moisture budget diagnosis

The total moisture tendency [Eq. (1)] at a constant pressure level is determined by the sum of horizontal and vertical moisture advections and the atmospheric apparent moisture sink Q_2 (Yanai et al. 1973):

$$\frac{\partial q}{\partial t} = -\mathbf{V}\cdot\nabla q - \omega\frac{\partial q}{\partial p} - \frac{Q_2}{L}, \tag{1}$$

where q is the specific humidity, t is the time, $\mathbf{V}$ is the horizontal wind vector, ∇ is the horizontal gradient operator, p is the pressure, ω is the vertical pressure velocity, Q_2 is the atmospheric apparent moisture sink, and L is the latent heat of condensation. The vertical advection term may be further decomposed into the horizontal moisture convergence term ($-q\nabla\cdot\mathbf{V}$) and the vertical flux term ($-\partial\omega q/\partial p$).

Applying a MJO-filtering operator (denoted by a prime) to the above moisture tendency equation, one may derive the intraseasonal moisture budget equation as the following:

$$\frac{\partial q'}{\partial t} = -(\mathbf{V}\cdot\nabla q)' - (q\nabla\cdot\mathbf{V})' - \frac{\partial}{\partial p}(\omega q)' - \frac{Q_2'}{L}. \tag{2}$$

The first term in the right-hand side of Eq. (2) represents the horizontal advection of moisture, the second term the horizontal moisture convergence, the third term the flux form of vertical moisture advection, and the fourth term moisture loss (gain) due to the condensational heating (raindrop-induced evaporation in the unsaturated atmosphere and surface evaporation) processes. The combination of second and third terms represents the vertical advection of moisture.

To identify the relative contribution of eddy–eddy and eddy–mean flow interactions, we decompose each variable into a LFBS (>90 day) component, a 20–80-day intraseasonal component, and a 3–10-day synoptic-scale component. For example, specific humidity may be decomposed into

$$q = \overline{q} + q' + q^*,$$

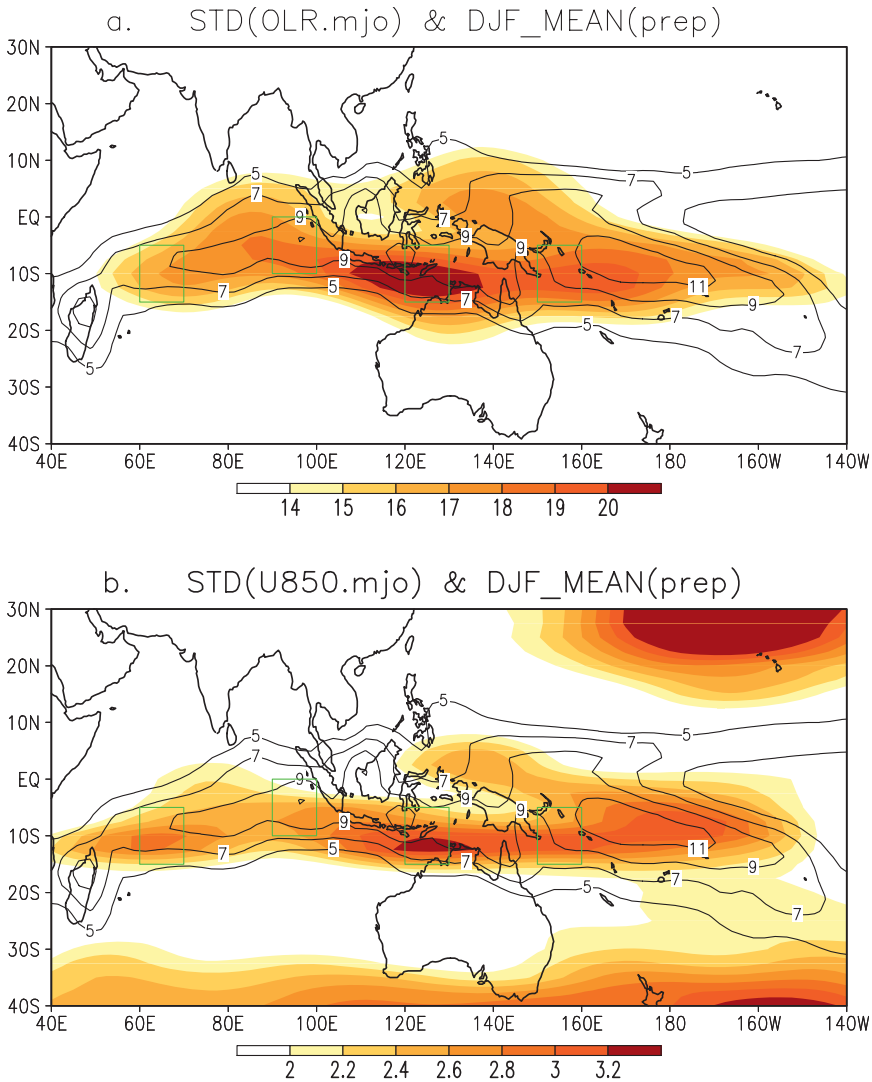

FIG. 1. (a) Standard deviation of MJO-filtered OLR (shading, W m^{-2}) and mean precipitation (contour, mm day^{-1}) during DJF of 1979–2001. (b) As in (a), but the shading represents the standard deviation of MJO-filtered zonal wind (m s^{-1}). Green boxes present the four MJO activity centers.

where an overbar, a prime, and an asterisk denote the LFBS, MJO, and synoptic-scale component, respectively. Our calculations show that the amplitude of high-frequency synoptic variability averaged over a MJO period is close to zero [i.e., $(q^*)' \approx 0$ and $(\mathbf{V}^*)' \approx 0$] and that terms associated with synoptic eddy interactions with LFBS and MJO flows [$-(\overline{\mathbf{V}} \cdot \nabla q^*)'$, $-(\mathbf{V}' \cdot \nabla q^*)'$, $-(\mathbf{V}^* \cdot \nabla \overline{q})'$, and $-(\mathbf{V}^* \cdot \nabla q')'$] are 3–4 orders of magnitude smaller than the sum of all moisture advection terms. Similarly, the contributions of the LFBS–eddy and MJO–eddy interaction terms [$-(\overline{q}\nabla \cdot \mathbf{V}^*)'$, $-(q'\nabla \cdot \mathbf{V}^*)'$, $-(q^*\nabla \cdot \overline{\mathbf{V}})'$ and $-(q^*\nabla \cdot \mathbf{V}')'$] to the total MJO moisture convergence are negligible. Thus, to the first-order of approximation, the horizontal moisture advection and convergence terms can be written as

$$-(\mathbf{V} \cdot \nabla q)' \approx -(\overline{\mathbf{V}} \cdot \nabla q')' - (\mathbf{V}' \cdot \nabla \overline{q})' - (\mathbf{V}' \cdot \nabla q')' - (\mathbf{V}^* \cdot \nabla q^*)', \quad \text{and} \tag{3}$$

$$-(q\nabla \cdot \mathbf{V})' \approx -(\overline{q}\nabla \cdot \mathbf{V}')' - (q'\nabla \cdot \overline{\mathbf{V}})' - (q'\nabla \cdot \mathbf{V}')' - (q^*\nabla \cdot \mathbf{V}^*)'. \tag{4}$$

A power spectrum analysis shows that the LFBS, MJO, and synoptic variability are well separated in the most of tropical regions. The examination of Eqs. (3)

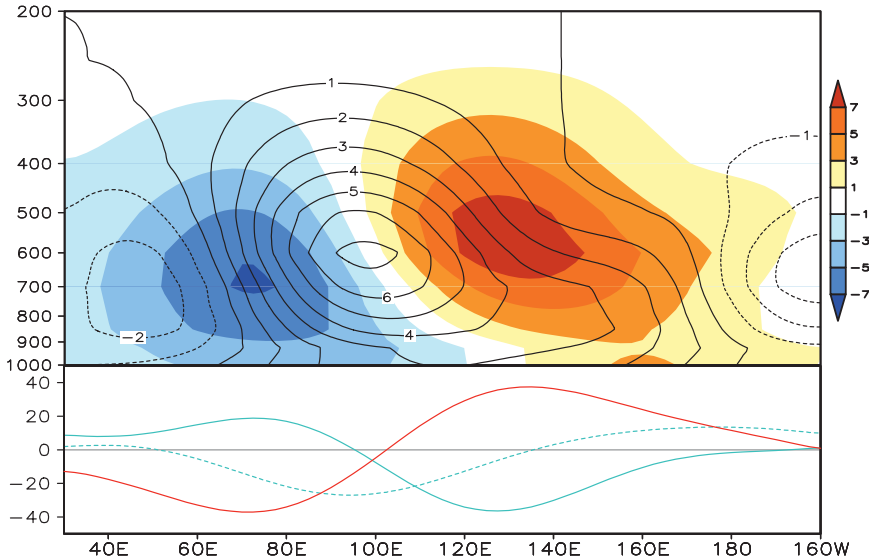

FIG. 2. (top) Zonal–vertical distributions of 0°–10°S-averaged MJO-filtered specific humidity (contour, 10^{-4} kg kg^{-1}) and specific humidity tendency (shading, 10^{-10} kg kg^{-1} s^{-1}). (bottom) Zonal distributions of 0°–10°S-averaged MJO-filtered OLR (blue dashed line, W m^{-2}), OLR tendency (blue solid line, 10^{-6} W m^{-2} s^{-1}), and column-integrated specific humidity tendency (red line, 10^{-7} kg m^{-2} s^{-1}) during the active phase of MJO in the EIO.

and (4) may help us to reveal explicitly to what extent the MJO flow alone and its interaction with the LFBS and synoptic eddy may contribute to the observed MJO moisture structure and evolution.

3. Cause of PBL moisture asymmetry relative to MJO convection

The MJO moisture–convection phase relationship during the peak phase of MJO in the eastern equatorial Indian Ocean was first examined. Figure 2 illustrates the composite zonal–vertical distribution of MJO-filtered moisture and its phase relationship with the MJO convection (represented by a negative OLR center). While in the middle troposphere the maximum moisture anomaly is collocated with the MJO convection, in the PBL there is a clear zonal asymmetry in the perturbation moisture field, that is, a positive (negative) center is located to the east (west) of the OLR center. Because of this asymmetry, the maximum moisture content line tilts eastward and downward. This moisture tilting feature was previously identified by Sperber (2003) and Kiladis et al. (2005).

As shown in Fig. 2, the MJO moisture at the PBL is enhanced (suppressed) to the east (west) of the MJO convection. To demonstrate how the PBL moisture asymmetry affects the MJO growth and evolution via atmospheric destabilization, the vertical profile of the intraseasonal equivalent potential temperature (θ_e') is examined. The equivalent potential temperature (θ_e) depends on both the specific humidity and temperature profiles of actual atmosphere. If a layer of air mass is initially moist but unsaturated and within the layer $\partial\theta_e/\partial z < 0$, then we call the layer of the atmosphere being potentially (or convectively) unstable. If such a layer is brought to saturation by sufficient lifting, the whole layer becomes actually unstable (Holton 1992; Emanuel 1994). The occurrence of deep convection (such as thunderstorm) is often preceded by a period when the atmosphere is potentially unstable (Houze 1993).

As shown in the top panel of Fig. 3, a significant increase of low-level θ_e' is found, consistently with PBL moistening, to the east of the MJO convection. If defining a convective instability parameter as the difference of θ_e' between the PBL (850–1000 hPa) and the middle troposphere (400–500 hPa), one may find that the atmosphere is more (less) potentially unstable to the east (west) of the MJO convective center (bottom panel of Fig. 3). Therefore, a phase leading of a positive low-level moisture anomaly may set up a relatively unstable stratification and generate a favorable environment for potential development of new convection to the east of the MJO convection center.

The westward tilting of moisture with height to the east of the convection implies that for an observer at a fixed location, the moisture precursor signal first appears in low level, and then moves upward. This is consistent with the fact that shallow convection and cumulus congestus clouds appear prior to MJO deep convection

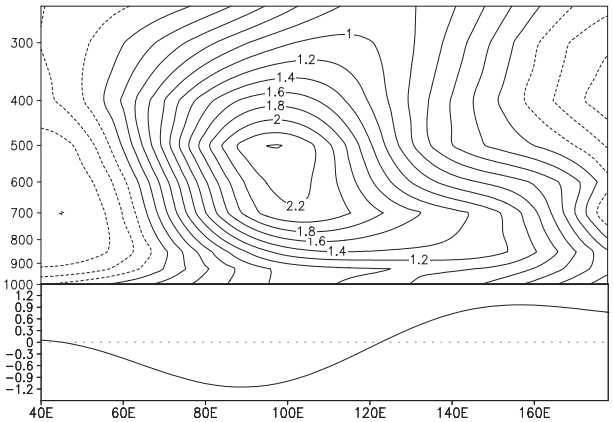

FIG. 3. As in Fig. 2, but for (top) MJO-filtered equivalent potential temperature (θ_e') and (bottom) the convective instability index , which is defined as the difference of θ_e' at the PBL and the middle troposphere [i.e., 1000–850-hPa averaged θ_e' minus 500–400-hPa averaged θ_e']. Unit: K.

(Johnson et al. 1999; Kikuchi and Takayabu 2004; Benedict and Randall 2007). The shallow convection transports moisture upward to moisten/warm the middle troposphere. The deep convection is then triggered when the midtropospheric moisture reaches its maximum (Kemball-Cook and Weare 2001; Kikuchi and Takayabu 2004; Benedict and Randall 2007). This implies that the midtroposphere moisture is conducive to deep convection (e.g., Brown and Zhang 1997; Sherwood 1999; Bretherton et al. 2004; Takayabu et al. 2006; Holloway and Neelin 2009). The increase of the midtropospheric moisture, on one hand, generates condensation heating to maintain the deep convection and on the other hand adjusts the atmospheric stratification to a more stable stratification. This relatively stable condition in the lower to middle troposphere is reflected by the anomalous negative potential instability index over the MJO convection region (Fig. 3). Thus, a key element to understand the MJO eastward propagation is to reveal specific processes that cause the PBL moistening ahead of MJO convection.

To examine what causes the PBL moistening, we will conduct a PBL-integrated moisture budget diagnosis. Some previous studies (e.g., M09) diagnosed a column-integrated moisture budget. As shown in Fig. 2, this column-integrated tendency is in phase with the moisture tendency in the middle troposphere and thus it may primarily reflect the moisture change in the midtroposphere. While we agree that the midtropospheric moistening is important for deep convection (e.g., Brown and Zhang 1997; Sherwood 1999; Bretherton et al. 2004; Takayabu et al. 2006; Holloway and Neelin 2009), we argue that the midtropospheric moistening associated with MJO is a result of shallow convections caused by the potential instability of lower troposphere. The argument is supported by the schematic diagram in Fig. 4 (from Benedict and Randall 2007). At a fixed location, the precursor moisture signal first shows up in PBL during day −20 to day −10. The PBL moistening destabilizes lower troposphere and triggers shallow convection. This leads to the deepening of moist layer, which eventually induces the onset of MJO deep convection (at day −10 to day −5). At day 0, stratiform anvil clouds dominate, as the OLR reaches its minimum (Fig. 4). Because of the stepwise processes, maximum OLR tendency lags the PBL moistening.

Before diagnosing the PBL moisture budget, we examine 3D circulation patterns associated with MJO to show the appropriateness of the current MJO index. The circulation pattern will also help us to understand how the MJO flow contributes to moistening processes in the later analysis. The circulation anomalies at 200 and 850 hPa associated with the MJO convection over the EIO were displayed in Fig. 5. It generally shows a baroclinic Rossby–Kelvin wave couplet structure in response to the MJO heating, similar to that described in Hendon and Salby (1994) and Salby et al. (1994). To the west of the MJO convection, there are two large-scale anticyclonic (cyclonic) Rossby wave gyres in the upper (lower) troposphere at both sides of the equator, accompanied with pronounced easterly (westerly) flows near the equator. To the east of the MJO convection, westerly (easterly) flows associated with the Kelvin wave response appear in the upper (lower) troposphere. Both the OLR center and the wave couplet structure shift slightly to the south of the equator, as the seasonal mean precipitation center in the region is primarily confined to the south of the equator (Li and Wang 1994). The circulation anomalies at 1000 hPa (not shown) in general resemble those at 850 hPa.

The zonal–vertical distributions of MJO circulations show a dominant first baroclinic mode vertical structure in the zonal and meridional wind fields (Fig. 6). At and to the west of the MJO convection, the westerly is pronounced in the lower-to-middle troposphere, while the easterly appears above 300 hPa. The maximum westerly appears around 850 hPa, and the zonal wind tilts westward with height. A similar tilting is found to the east of the MJO convection (Fig. 6a). A northerly (southerly) flow is observed in the vicinity of the MJO convection in the lower (upper) troposphere (Fig. 6b). As shown in the following, this meridional wind plays a role in anomalous moisture advection. While the strongest upward motion appears in the middle troposphere and is in phase with the OLR minimum center (90°–100°E), at top of the PBL the ascending anomaly tends to prevail to the east of the MJO convection (Fig. 6c). As a result, the vertical motion

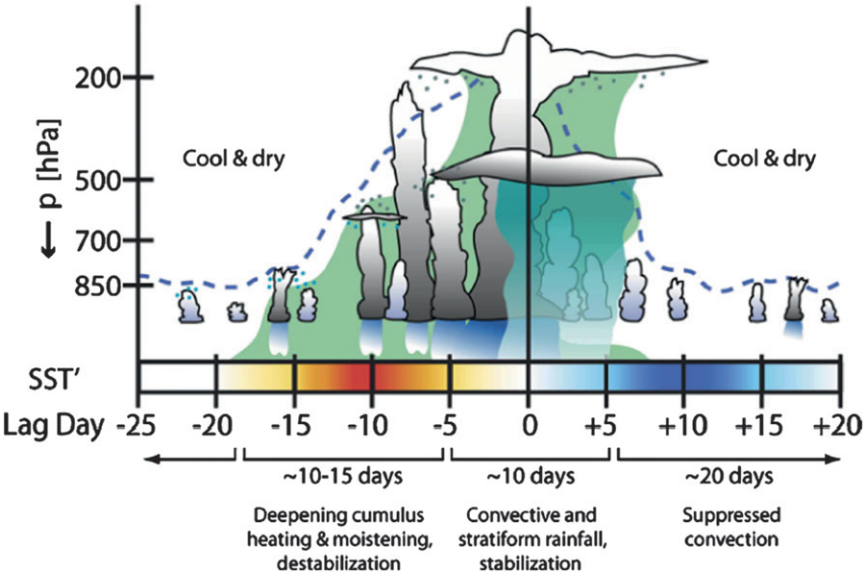

FIG. 4. Schematic diagram illustrating temporal phase relationships among anomalous moisture, shallow convection, and deep convection associated with the MJO. The horizontal axis denotes lagged days relative to the day of maximum rainfall (day 0). The vertical axis is the pressure. The approximate cloud top is indicated by the dashed blue line, while green shading represents the general area of positive moisture anomalies. Light blue dots above shallower convective clouds represent moistening via detrainment, while gray dots below stratiform cloud types represent ice crystal fallout and moistening. (from Benedict and Randall 2007).

associated with MJO also tilts eastward as height decreases. The asymmetry of the vertical motion at top of the PBL is dynamically consistent with the divergence field at the PBL, which also reveals a remarkable zonal asymmetry with a convergence (divergence) appearing to the east (west) of the MJO convection (Fig. 6d). As demonstrated in the subsequent moisture budget analysis, the zonal asymmetry of the PBL divergence is essential to cause the moisture asymmetry in the boundary layer.

To reveal the cause of the moisture asymmetry, a vertical (1000–700 hPa) integrated MJO moisture budget analysis was performed over the PBL moistening region of (130°–150°E, 0°–10°S). Figure 7a shows the contribution from each of the moisture budget terms. The largest positive contribution is the vertical moisture advection term. The cause of the positive vertical advection is primarily due to the advection of the mean moisture (which has a maximum at the surface and decays exponentially with height) by anomalous ascending motion, the latter of which is associated with the PBL convergence. If one separates the vertical advection term into a horizontal moisture convergence term $[-(q\mathbf{V}\cdot\mathbf{V})']$ and a vertical flux term $[-\partial(\omega q)'/\partial p]$, one may find that the two terms are somehow offset with each other, with the moisture convergence term $[-(q\nabla\cdot\mathbf{V})']$ dominating the vertical flux term. This indicates that the boundary layer convergence and associated ascending motion play an important role in moistening the PBL to the east of deep convection. In addition to the convergence effect, the horizontal moisture advection $[-(\mathbf{V}\cdot\nabla q)']$ also contributes to the PBL moistening, although its magnitude is 5 times smaller than the vertical moisture advection term. Our result is consistent with Benedict and Randall (2007) who indicated that increased moisture convergence and advective processes are crucial for supporting MJO convection. The term $-Q_2'/L$ tends to reduce the moistening in the lower troposphere. The negative anomaly of $-Q_2'/L$ in PBL (1000–700 hPa) results from the shallow convection–induced precipitation and the reduction of the surface evaporation ahead of MJO convection. The sum of all terms in the right-hand side of Eq. (2) is close to the observed MJO moisture tendency.

We next examine specific processes that give rise to the positive moisture tendency. Figure 7b shows major terms related to the moisture convergence. The leading term comes from the convergence of the mean moisture by the MJO flow [i.e., $-(\overline{q}\nabla\cdot\mathbf{V}')'>0$]. This process accounts for 88% of the total moisture convergence contribution. A further diagnosis shows that the enhanced MJO zonal wind convergence ($-\partial u'/\partial x>0$) accounts largely for this positive moisture tendency, whereas the divergence of the MJO meridional wind ($-\partial v'/\partial y<0$) induces a negative tendency. This seems

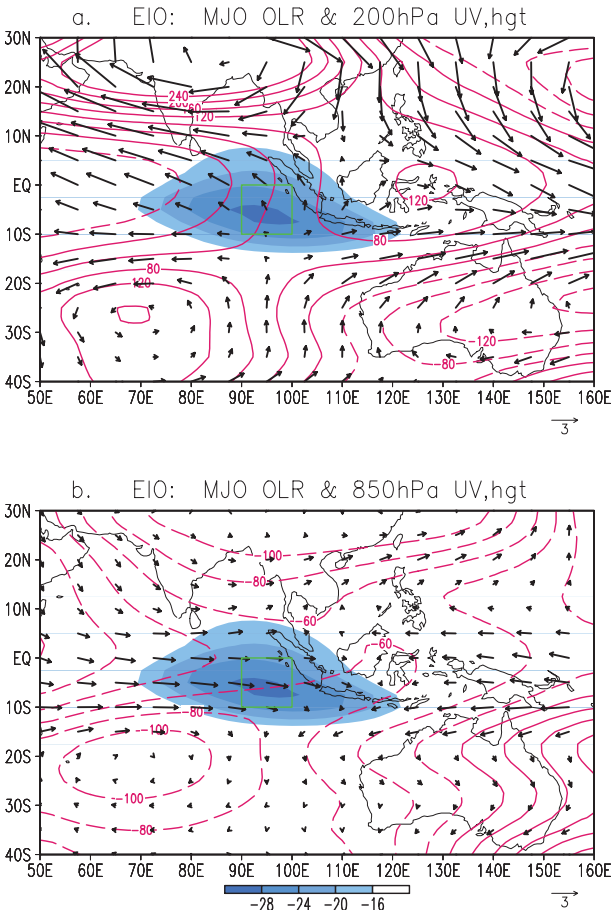

FIG. 5. Composites of MJO-filtered OLR (shading, W m^{-2}), geopotential (contour, m^2 s^{-2}), and wind fields (vector, m s^{-1}) at (a) 200 and (b) 850 hPa during the active phase of MJO in the EIO (green boxes).

different from the conventional frictional wave–CISK theory (Wang 1988; Wang and Li 1994), which shows an equatorially symmetric feature with a convergent meridional wind component ahead of the convection. In the current analysis, the maximum MJO convection shifts to the south of the equator because of the asymmetry of the boreal winter mean climate. The term $[-(q'\mathbf{\nabla}\cdot\overline{\mathbf{V}})']$, the mean convergence of the anomalous moisture, also plays a role in the MJO moistening. It accounts for about 10% of the total MJO moisture convergence contribution.

The much greater contribution of $-(\overline{q}\mathbf{\nabla}\cdot\mathbf{V}')'$ than $-(q'\mathbf{\nabla}\cdot\overline{\mathbf{V}})'$ is primarily attributed to the large difference between the mean and intraseasonal moisture amplitude. The mean moisture ($\overline{q}$) is about 40 times larger than the MJO moisture (q') to the east of the convection. At the same region, however, the mean convergence ($\mathbf{\nabla}\cdot\overline{\mathbf{V}}$) is only about 10 times larger than the MJO convergence ($\mathbf{\nabla}\cdot\mathbf{V}'$). Because both the moisture and convergence perturbations associated with MJO are relatively small, the product of the two $[-(q'\mathbf{\nabla}\cdot\mathbf{V}')']$ is negligible (Fig. 7b). In addition, the contribution of synoptic eddy moisture convergence $[-(q^*\mathbf{\nabla}\cdot\mathbf{V}^*)']$ is also negligible, accounting for less than 1% of the total MJO moisture convergence contribution (Fig. 7b).

The leading term in the MJO moisture advection is $[-(\mathbf{V}'\cdot\mathbf{\nabla}\overline{q})']$, which denotes the advection of the mean moisture by the MJO flow (Fig. 7c). The middle panel of Fig. 8 illustrates the spatial distributions of the mean moisture and MJO flows in association with zonal and meridional moisture advections. Over the maximum PBL moisture region (130°–150°E, 0°–10°S), the MJO easterly advecting the mean moisture is responsible for the positive moisture tendency in the region (Fig. 8b). The second leading term in the moisture advection is $[-(\overline{\mathbf{V}}\cdot\mathbf{\nabla}q')']$, which is associated with the anomalous moisture advection by the mean flow (Fig. 7c). Although the DJF mean westerly induces a negative zonal moisture advection (Fig. 8a), the mean northerly tends to produce a stronger positive meridional moisture advection (Fig. 8d). As a result, the net effect of $[-(\overline{\mathbf{V}}\cdot\mathbf{\nabla}q')']$ is positive. The third leading term is $[-(\mathbf{V}'\cdot\mathbf{\nabla}q')']$, which represents the anomalous moisture advection by the anomalous flow. Note that a positive $[-(\mathbf{V}'\cdot\mathbf{\nabla}q')']$ is mainly contributed by the zonal component (Fig. 8c), which is partially offset by a weak negative meridional moisture advection associated with a weak MJO southerly (Fig. 8f).

It is worth noting that the moisture advection due to synoptic-scale eddy–eddy interactions $[-(\mathbf{V}^*\cdot\mathbf{\nabla}q^*)']$ produces a negative MJO moisture tendency (Fig. 7c). A further diagnosis shows that both the zonal and meridional components of the eddy moisture advection exhibit a negative contribution (figure not shown). This indicates that the nonlinear eddy moisture advection does not play a role in contributing to the PBL moistening over the EIO. This result seems different from the modeling study of M09, who emphasized the effect of the synoptic eddy moisture advection on MJO activity around 155°E. Is the inconsistence simply attributed to the model bias or does it reflect a geographically dependent feature? A further comparison of the moisture processes in different regions will be examined in section 5 to address this question.

4. Mechanisms for phase leading of the PBL convergence

In the previous section we revealed the phase leading of the PBL moisture ahead of the MJO convection. What causes the moisture asymmetry? Physically, two factors may contribute to the moisture change. The first factor

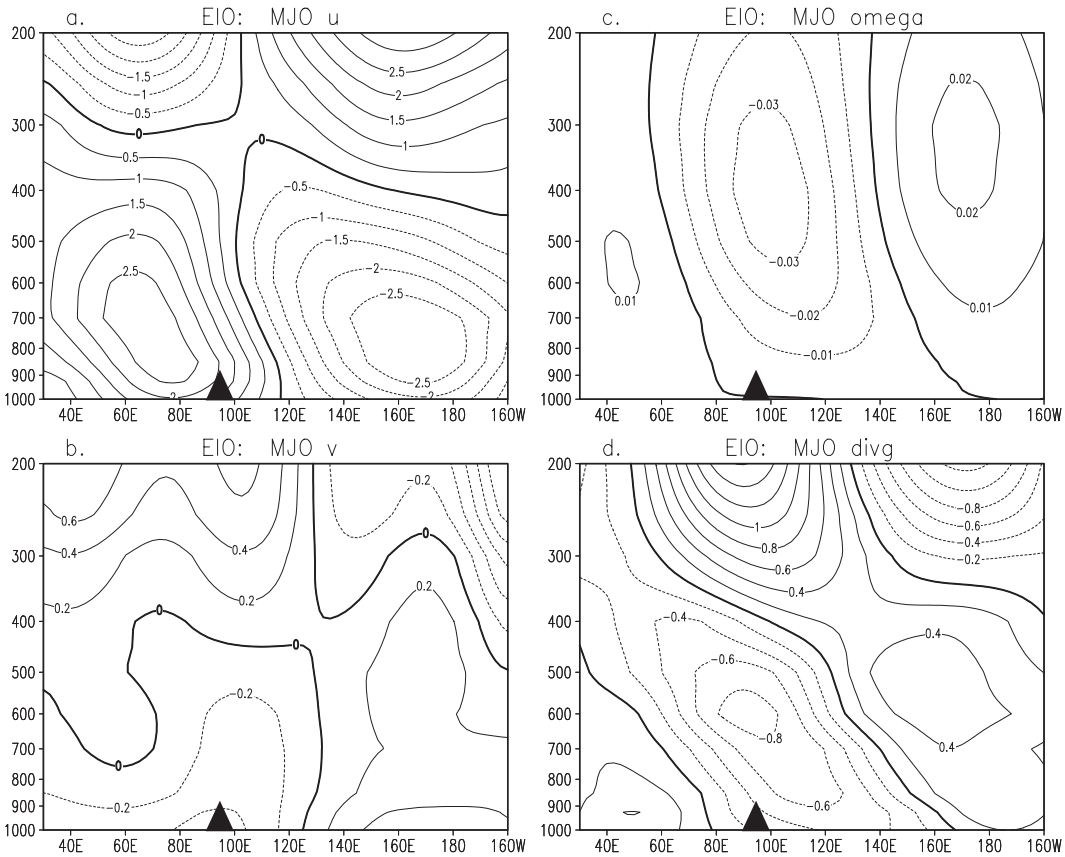

FIG. 6. Zonal–vertical distributions of 0°–10°S-averaged MJO-filtered (a) zonal wind (m s^{-1}), (b) meridional wind (m s^{-1}), (c) vertical velocity (pa s^{-1}), and (d) divergence (10^{-6} s^{-1}) for the MJO active phase in the EIO. The triangles indicate the MJO convection center.

is the boundary layer convergence, and the second factor is the surface evaporation. Our diagnosis shows that while the low-level convergence shows a significantly eastward shift to the MJO convection (Fig. 6d), the surface evaporation tends to decrease to the east of MJO convection (Fig. 9). Here the surface evaporation fields derived from the ERA-40, the OAFlux, and the bulk formula all show a consistent result with a decreased (increased) evaporation the east (west) of the MJO convection. This indicates that the boundary layer convergence is a major process that causes the observed phase leading of PBL moisture.

The decrease of the surface evaporation or upward latent heat flux (LHF) is attributed to the decrease of the surface wind speed. In the southeastern Indian Ocean where the mean westerly flow prevails, the intraseasonal easterly (westerly) to the east (west) of MJO convection suppresses (enhances) the surface wind speed and thus leads to a suppressed (enhanced) LHF. The change of the LHF further leads to the change in SST (Jones and Weare 1996; Shinoda et al. 1998; Araligidad and Maloney 2008). As shown in Fig. 9, a warm (cold) SST anomaly (SSTA) due to the weaker (stronger) surface evaporation is observed to the east (west) of MJO convection.

How does the warm SSTA contribute to the eastward propagation? According to Lindzen and Nigam (1987), a warm SSTA may induce a boundary layer convergence through the change of the boundary layer temperature and pressure. However, it is not clear to what extent the observed PBL convergence is contributed by the underlying SSTA.

The effect of air–sea interactions on MJO eastward propagation has been mentioned by previous studies (e.g., Sperber et al. 1997; Waliser et al. 1999; Fu et al. 2003; Li et al. 2008), but specific processes that contribute to the eastward propagation are not clear. Here we intend to address the following two important questions: through what physical processes is the phase-leading PBL convergence generated, and to what extent does the warm SSTA in front of the convection contribute to the boundary layer convergence? Fig. 10 is a schematic diagram illustrating key processes that contribute to the phase leading of the boundary layer convergence. For simplicity, this schematic diagram displays an equatorially symmetric feature,

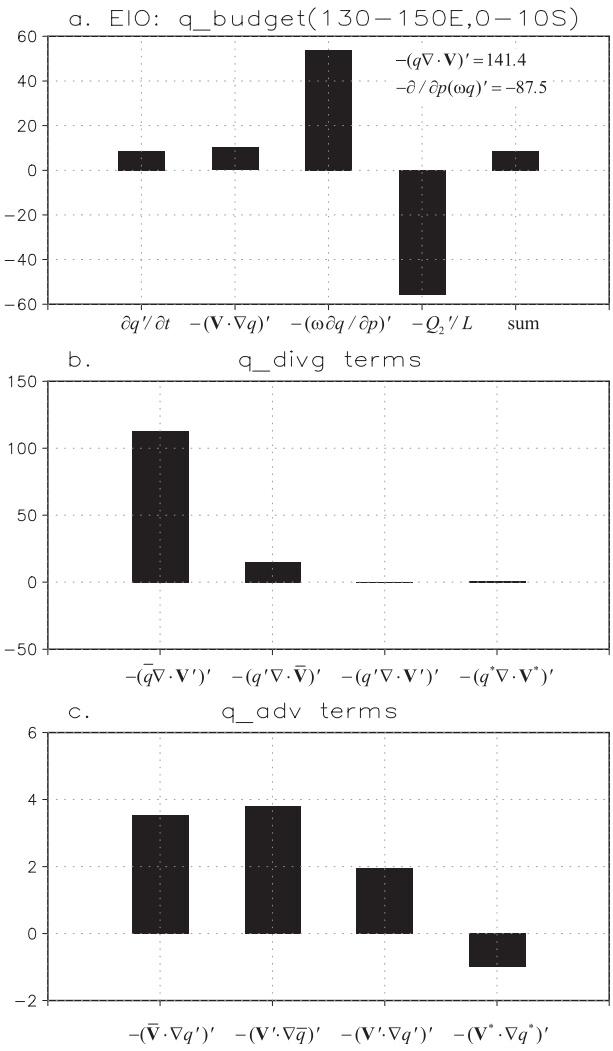

FIG. 7. (a) PBL (1000–700 hPa) integrated intraseasonal moisture budget terms over PBL moistening region of (130°–150°E, 0°–10°S). From left to right, observed specific humidity tendency, horizontal moisture advection, vertical moisture advection, latent heating, and sum of these budget terms are shown. The relative contributions of horizontal moisture convergence $[-(q\mathbf{V}\cdot\mathbf{V})']$ and vertical flux term $[-\partial(\omega q)'/\partial p]$ to the vertical moisture advection $[-(\omega\partial q/\partial p)']$ are shown inside the panel. (b) Individual components of the MJO moisture convergence. (c) As in (b), but for the MJO moisture advection process. Unit is 10^{-7} kg m^{-2} s^{-1}.

although in reality the circulation may shift slightly south of the equator in boreal winter. First, the midtropospheric heating associated with MJO deep convection induces a baroclinic free-atmosphere response, with a Kelvin (Rossby) wave response to the east (west) of the convective center. The anomalous low pressure at top of the PBL associated with the Kelvin wave response may induce a convergent flow in the boundary layer, while a PBL divergence may occur to the west of the convective center between two Rossby wave gyres. Thus the first convergence-generation process is associated with the midtropospheric heating and equatorial wave responses to the heating. The second generation process is associated with the SSTA forcing. As a warm SSTA is generated to the east of the MJO convection, the warm SSTA may drive boundary layer flows through induced hydrostatic effect on sea level pressure (Lindzen and Nigam 1987). Therefore, the convergence in the atmospheric boundary layer may be connected to the underlying positive SST anomaly and associated SSTA gradients to the east of the MJO convection.

To examine quantitatively the relative roles of the SSTA gradient–induced pressure gradient force and the heating-induced free-atmospheric wave dynamics in determining the PBL convergence, we diagnose the boundary layer momentum budget equation developed by Wang and Li (1993). The PBL momentum Eq. (2.21) in Wang and Li (1993) states

$$f\mathbf{k}\times\mathbf{V}_B' + E\mathbf{V}_B' = -\nabla\phi_e' + \frac{R}{2}\frac{(p_s - p_e)}{p_e}\nabla T_s', \qquad (5)$$

where a prime denotes the MJO component, f is the Coriolis parameter, $\mathbf{k}$ is the unit vector in the vertical direction, $\mathbf{V}_B$ denotes the vertically averaged horizontal wind in the boundary layer, ∇ is the horizontal gradient operator, ϕ_e denotes the geopotential at the top of the boundary layer, R is the gas constant of air, p_s and p_e are pressures at the bottom and top of the PBL, respectively, T_s is the surface temperature, and E is the friction coefficient and is equal to 10^{-5} s^{-1}. The first term in the right-hand side of Eq. (5) represents the free-atmospheric wave effect. The second term in the right-hand side of Eq. (5) represents the SSTA forcing effect. To test the sensitivity of the result to the boundary layer depth, two different PBL depths, 1000–850 hPa and 1000–700 hPa, are applied.

The vector form of Eq. (5) may be decomposed into two scalar equations for the zonal and meridional components, with the sum of two linear forcing terms. Once the zonal and meridional wind components are derived, the PBL divergence can be readily solved with either of the individual forcing terms. Figure 11 reveals the diagnosis results for the PBL convergence. It turns out that the free atmospheric wave effect in response to the MJO heating plays a major role in determining the boundary layer convergence. It accounts for 90% and 75% of the total boundary layer convergence in the case of p_e = 850 and p_e = 700, respectively. The warm SST anomaly induced by decreased LHF ahead of MJO convection, on the other hand, also plays a role. It contributes about 10%–25% to the observed boundary layer convergence. Since the PBL convergence is a major

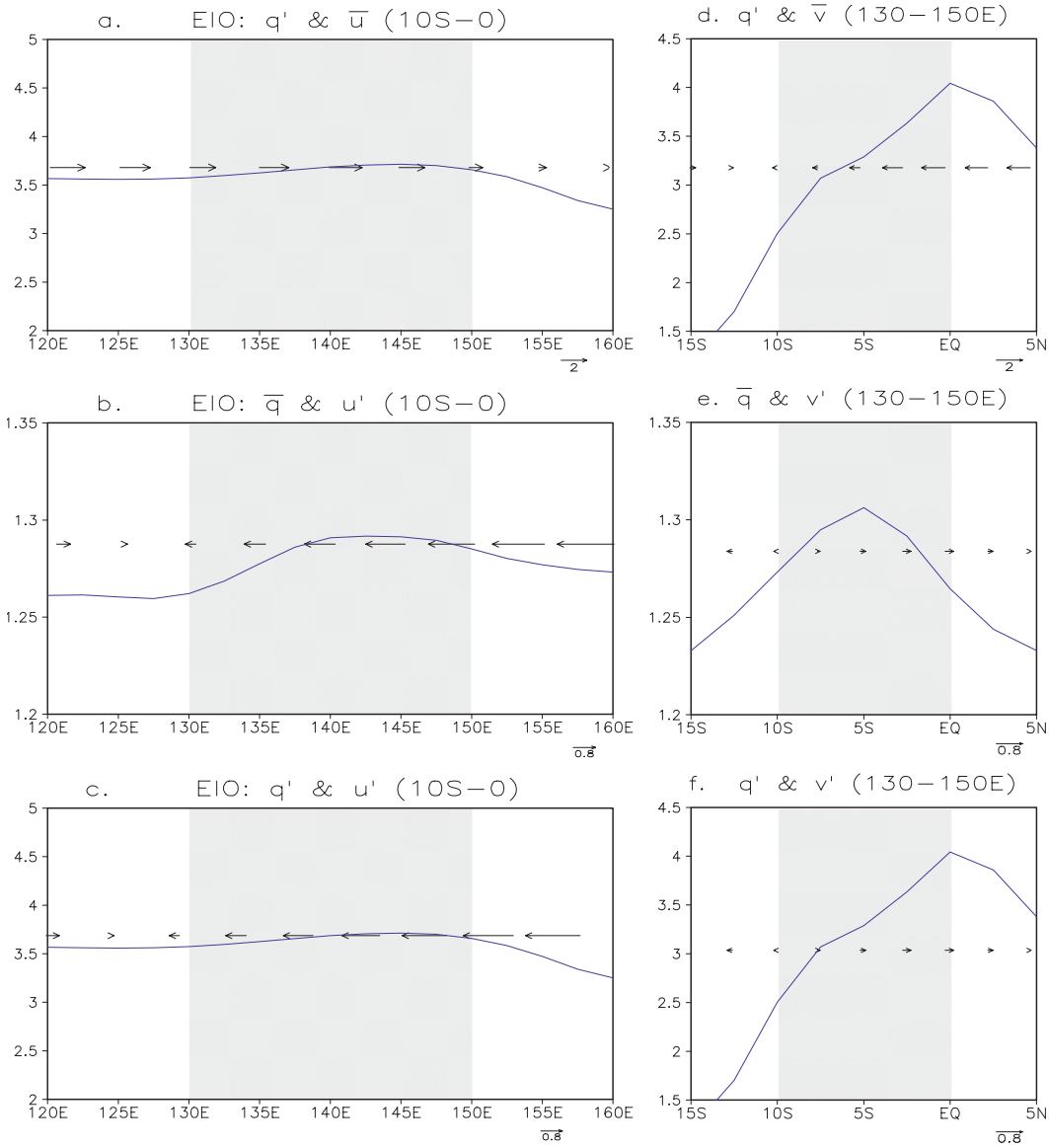

FIG. 8. (left) Zonal variations of 1000–700-hPa-averaged (a) MJO specific humidity (blue line, 10^{-4} kg kg^{-1}) and LFBS zonal wind (vector, m s^{-1}), (b) LFBS specific humidity (blue line, 10^{-2} kg kg^{-1}) and MJO zonal wind (vector, m s^{-1}), and (c) MJO specific humidity (blue line, 10^{-4} kg kg^{-1}) and zonal wind (vector, m s^{-1}) along 0°–10°S. (right) As on the left, but for the meridional variations of specific humidity and meridional wind along 130°–150°E. Shadings mark the MJO moisture advection diagnosis region.

factor affecting the moisture asymmetry, the result above suggests that both the heating-induced equatorial wave response and the underlying SSTA contribute to the eastward propagation of MJO.

5. MJO moisture budget diagnoses in WIO, MC, and WP

In the previous sections we focused on the MJO activity over the EIO. Given that the DJF mean states vary over the vast area of the Indian and Pacific Oceans and the MJO also experiences its initiation, mature, and weakening phases, it is necessary to examine the similarities and differences of MJO moisture dynamics associated with MJO development and propagation in the WIO, MC, and WP.

Similar to the MJO pattern shown in Fig. 5b, an anomalous low-level Rossby–Kelvin wave couplet is found in the WIO, MC, and WP regions, although the wind amplitudes vary and are a function of the intensity

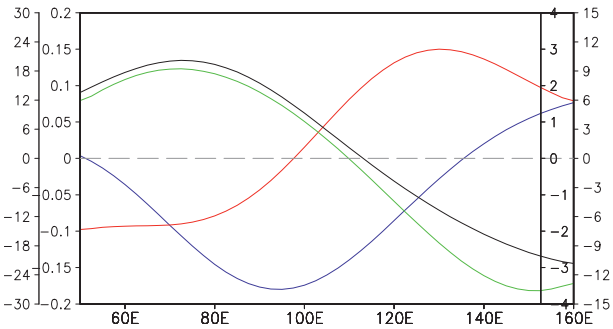

FIG. 9. Zonal variations of 0°–10°S averaged MJO-filtered OLR (blue, leftmost vertical axis, W m^{-2}), SST (red, left vertical axis, K), LHF (green, rightmost vertical axis, W m^{-2}), and zonal wind (black, right vertical axis, m s^{-1}) for the MJO active phase in the EIO. The LHF is based on the ensemble average of the ERA-40, OAFlux, and bulk formula.

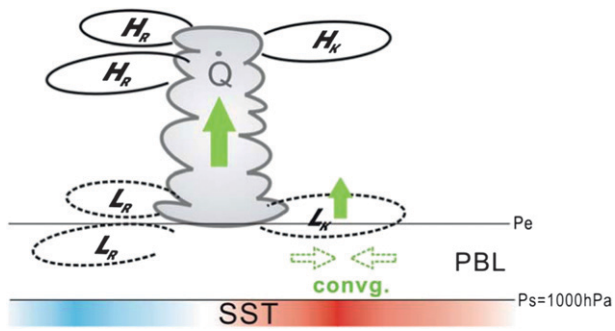

FIG. 10. Schematic diagram of boundary layer convergence induced by free-atmospheric wave dynamic and SST anomaly. Cloud stands for the MJO convection with heating, solid (dashed) gyres with H_K (L_K) and H_R (L_R) indicate the high (low) pressure anomaly associated with Kelvin and Rossby waves response to convection, respectively, red and blue shadings denote the positive and negative SST anomalies, respectively, solid green arrows indicates the anomalous ascending motion, dashed green arrows represent the boundary layer convergence, and Ps and Pe are pressure levels at the bottom and top of the PBL, respectively.

of the convection (Fig. 12). The low-level circulation is dominated by two cyclonic Rossby wave gyres, resided to the northern and southern parts of the OLR center. Because of the southward shift of mean convection in DJF, the cyclonic anomaly in the southern part tends to be stronger than that in the northern part. Along 10°S, the enhanced westerly associated with the Rossby wave response and the easterly associated with the Kelvin wave response converge onto the east of the OLR center. Thus the current ERA-40 analysis results show that the enhanced westerly penetrates through the MJO convective center in both the tropical Indian (Figs. 12a and 5b) and Pacific Oceans (Figs. 12b,c).

The vertical profiles of the MJO moisture, divergence, and zonal wind fields during its active phase were displayed in Fig. 13. The zonal asymmetric feature of the PBL moisture is also clearly presented in the WIO, MC, and WP regions (Figs. 13a,b,c). The greatest PBL moisture asymmetry appears during the mature phase of MJO in the MC region (Fig. 13b), as the boundary layer moisture shows a greatest eastward phase leading similar to that in the EIO (Fig. 2). The MJO divergence and zonal wind fields show a similar westward tilt with height in the three MJO active regions (see middle and right columns in Fig. 13).

The quantitative examination of each moisture budget term in the three regions is shown in Fig. 14. As expected, the leading term that contributes to the enhanced PBL moistening comes from the MJO moisture convergence process in all the regions. Even though the part of the moisture convergence is offset by the vertical moisture flux, the net effect of the two processes still dominates the PBL moisture budget in the WIO and WP (Figs. 14a,c). In the MC region, the net effect of the moisture convergence and the vertical flux is smaller than the horizontal moisture advection (Fig. 14b).

Table 1 lists individual term contributions associated with the moisture convergence and advection. It is noted that the convergence of the mean moisture by the MJO flow $[-(\overline{q}\nabla \cdot \mathbf{V}')' > 0]$ is dominant in the MJO moisture budget in all regions (Table 1). This is understandable since high mean moisture always appears over the Indian and Pacific warm pool. A boundary layer MJO convergence results in a much more efficient moisture convergence than the convergence of the perturbation moisture. The convergence of the DJF mean flow also favors the anomalous moisture convergence, particularly in the MC region (Table 1). The nonlinear terms associated with either MJO–MJO or

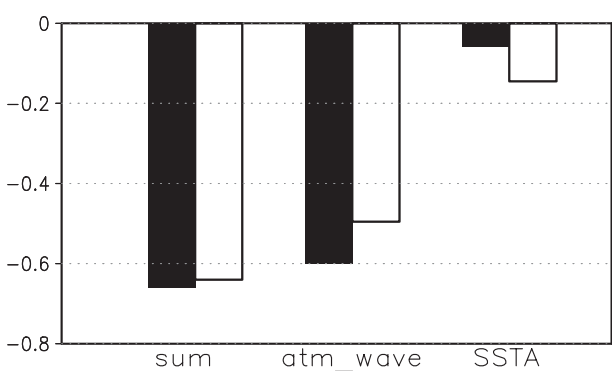

FIG. 11. From left to right, total boundary layer convergence averaged over (130°–150°E, 0°–10°S) induced by both the free-atmospheric wave dynamic and SST anomaly, and relative contributions of wave dynamic and SSTA effect in the case of p_e = 850 hPa (filled bars) and p_e = 700 hPa (hollow bars). Unit is 10^{-6} s^{-1}.

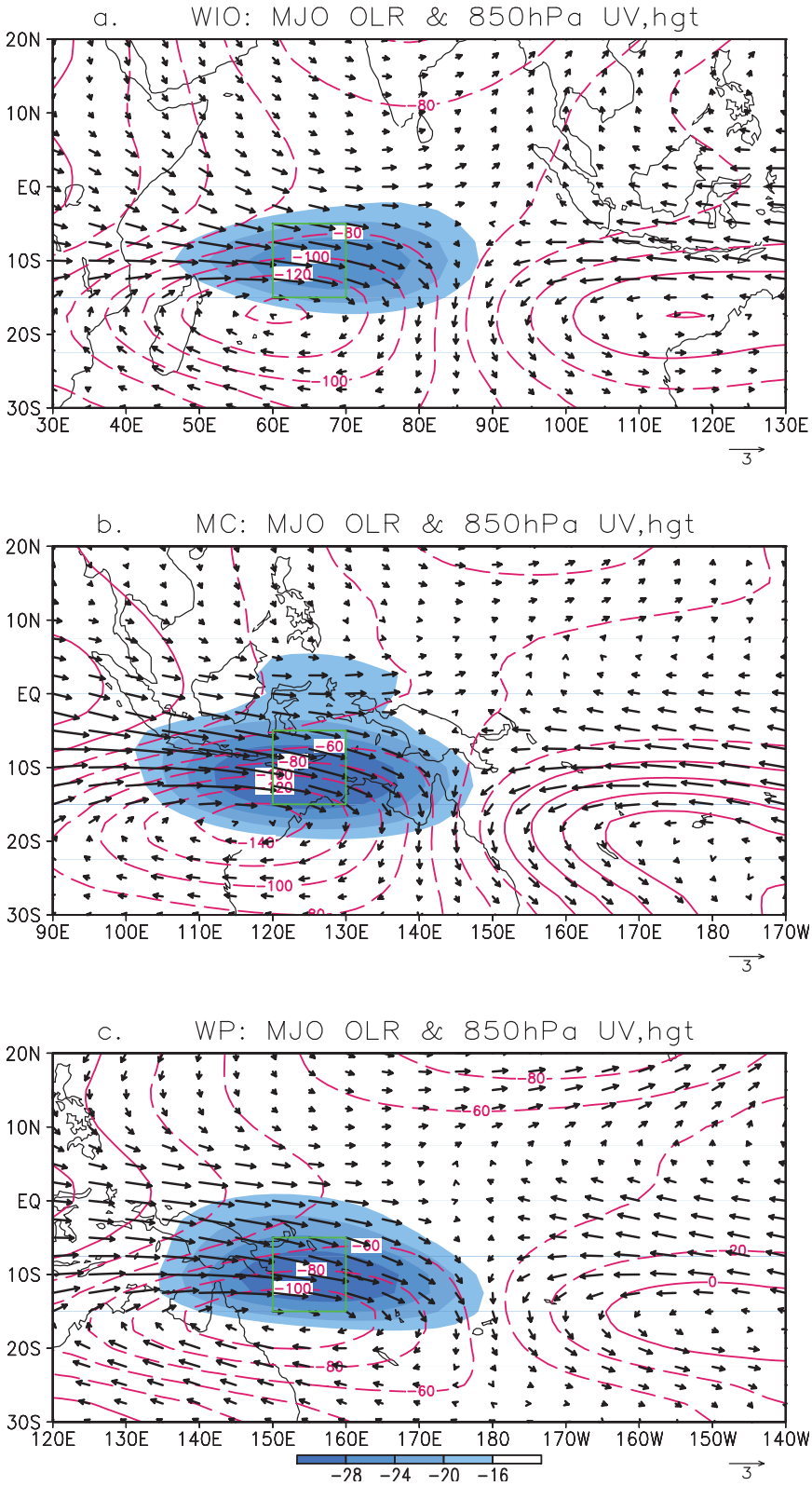

FIG. 12. As in Fig. 5b, but for the (a) WIO, (b) MC, and (c) WP MJO events.

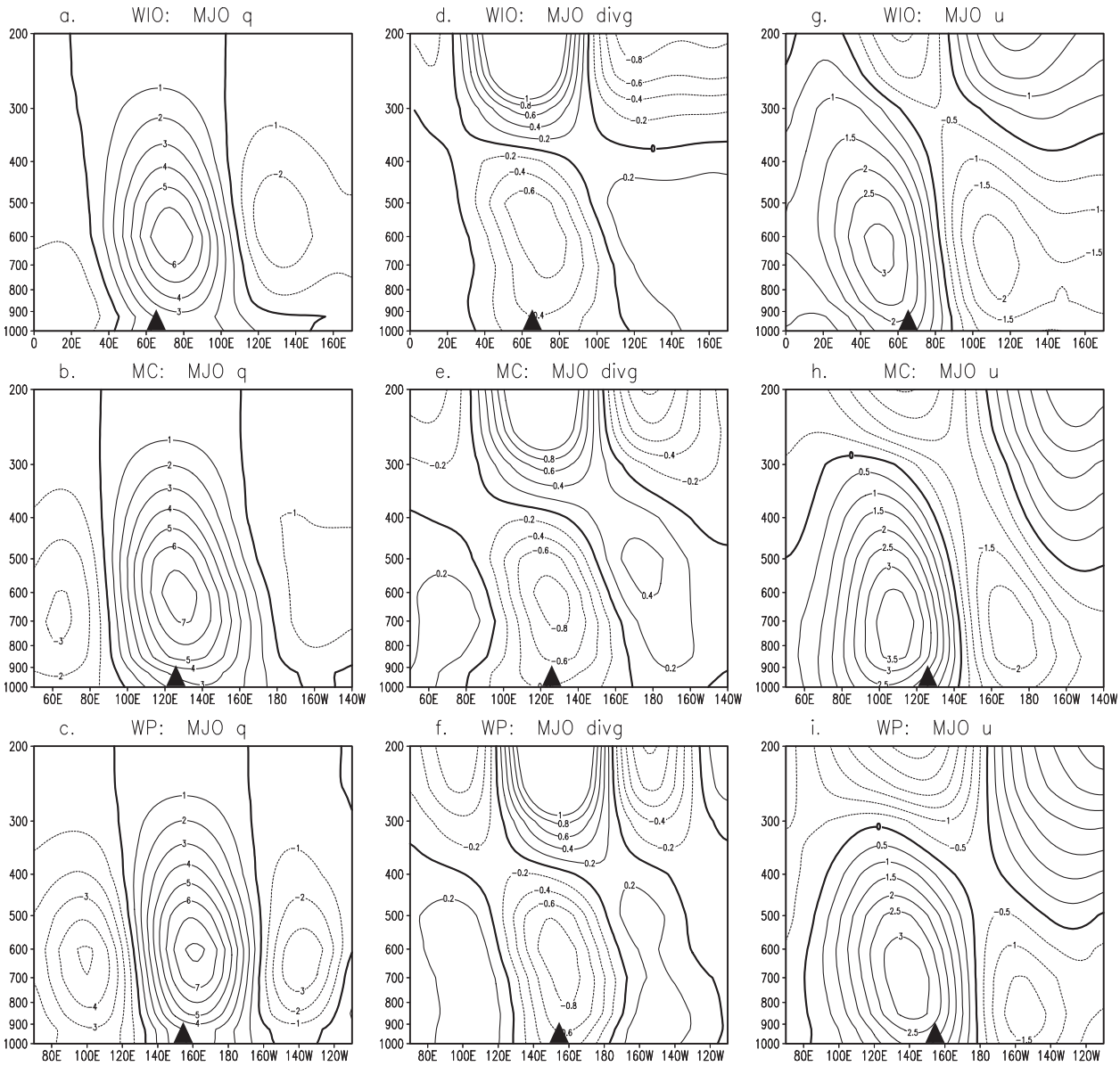

FIG. 13. Zonal–vertical distributions of 5°–15°S-averaged MJO-filtered specific humidity (kg kg^{-1}) for the MJO center in the (a) WIO, (b) MC, and (c) WP regions. (middle and right) As on the left, but for the divergence (10^{-6} s^{-1}) and zonal wind (m s^{-1}) fields, respectively. The triangles indicate the MJO convection center.

eddy–eddy interactions are generally small and negligible, and they even have a negative contribution in the MC region.

The diagnosis of MJO moisture advection shows a diverse result for different regions. In the WIO and MC, the MJO advection plays a secondary role in the boundary layer moistening (Figs. 14a,b), similar to that in the EIO. However, the moisture advection in the WP contributes negatively to the MJO moisture tendency (Fig. 14c). Despite of the difference above, the advection of mean moisture by the MJO flow $[-(\mathbf{V}' \cdot \nabla\overline{q})']$ is always a dominant term in all the MJO moisture advection terms for all regions (Table 1).

To examine the above advection process in detail, the zonal and meridional distributions of the mean moisture and the MJO flow are illustrated in Fig. 15. Since the zonal gradient of the mean moisture is very weak, the zonal advection term $(-u'\partial\overline{q}/\partial x)$ is relatively small in the WIO and MC. Because of the greater meridional gradient of the mean moisture, the MJO northerly induces a positive moisture tendency by advecting the maximum mean moisture from the equatorial region

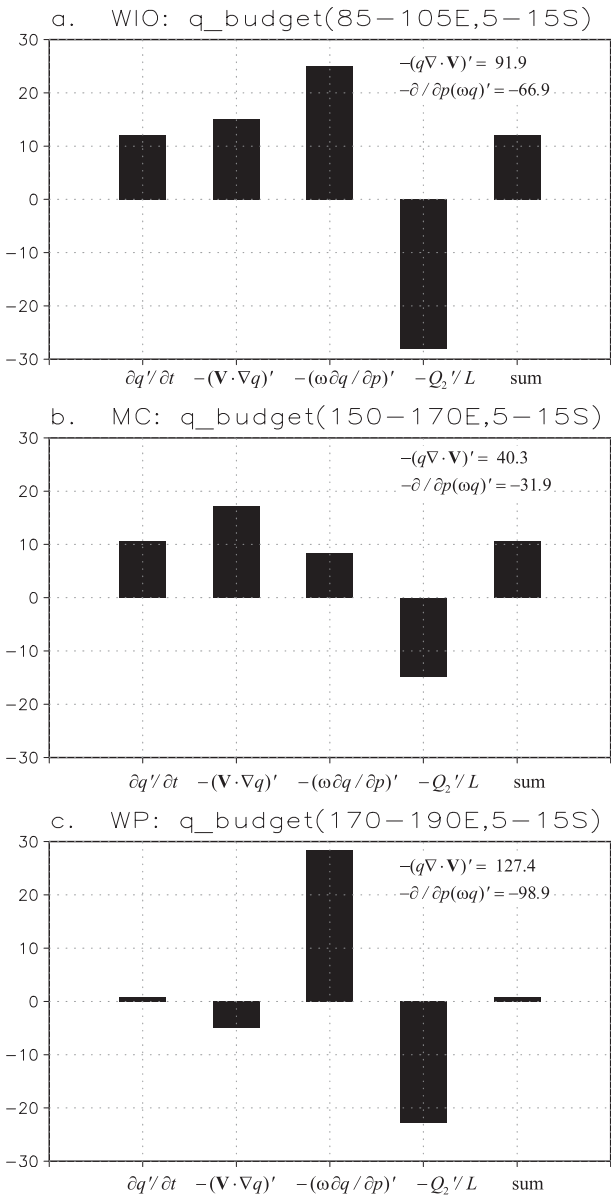

FIG. 14. As in Fig. 7a, but for the MJO convection in the (a) WIO, (b) MC, and (c) WP regions.

southward (Figs. 15d,e). In the WP, the zonal advection of the mean moisture by the MJO easterly leads to a negative moisture tendency contribution (Fig. 15c), which is offset by the positive moisture advection due to the MJO meridional wind (Fig. 15f, Table 1). In general, the advections of the perturbation moisture by the mean flow $[-(\overline{\mathbf{V}}\cdot\nabla q')']$ and by the MJO flow $[-(\mathbf{V}'\cdot\nabla q')']$ are relatively small and change greatly with space, compared to $[-(\mathbf{V}'\cdot\nabla\overline{q})']$ (Table 1). The finding in M09 that the synoptic eddy dominates MJO meridional moisture advection is geographically dependent. Table 1 shows that the eddy advection term $[-(\mathbf{V}^*\cdot\nabla q^*)']$ contributes positively to the MJO moisture tendency only over the MC region, and they are negative in other three regions.

6. Summary and discussions

The moisture dynamics responsible for the eastward propagation of MJO are examined through the MJO moisture budget diagnosis based on the ERA-40 reanalysis during DJF in 1979–2001. The precursor moisture signal first appears at the PBL (1000–700 hPa) ahead of the MJO convection. This moisture asymmetry leads to a potentially unstable stratification in the lower troposphere. With sufficient lifting because of PBL convergence, the potential instability may help trigger shallow convection. The shallow convection transports water vapor upward into the midtroposphere, leading to the onset of MJO deep convection. This stepwise development of MJO shallow-to-deep convection was previously identified (e.g., Kemball-Cook and Weare 2001; Kikuchi and Takayabu 2004; Benedict and Randall 2007). Therefore, the key element for the eastward propagation is the PBL moisture asymmetry relative to the MJO convection.

A moisture budget analysis was performed to understand the process that contributes to the PBL moisture asymmetry. The diagnosis result indicates that the vertical advection term or the horizontal moisture convergence term dominates the low-level moistening ahead of MJO convection. To separate the effect of the basic state, MJO perturbation and synoptic eddy, we partitioned each atmospheric field into the LFBS (>90 days), MJO (20–80 days), and synoptic (3–10 days) components. It is found that the term $[-(\overline{q}\nabla\cdot\mathbf{V}')']$ contributes about 80% of the total horizontal moisture convergence in all regions analyzed (from the western Indian Ocean to the western Pacific). This is because the mean moisture across the tropical Indian and Pacific warm pool is much greater than the perturbation moisture, and as a result the convergence of the background moisture by the MJO flow is much greater than the convergence of anomalous moisture by either the mean or MJO flow $[-(q'\nabla\cdot\overline{\mathbf{V}})'$ and $-(q'\nabla\cdot\mathbf{V}')']$. We note that the contribution by synoptic-scale moisture and convergence $[-(q^*\nabla\cdot\mathbf{V}^*)']$ is very small and accounts for about 3% of the total MJO moisture convergence.

The horizontal moisture advection also contributes to the PBL moistening ahead of MJO convection. The leading term in all four regions is associated with the advection of the mean specific humidity by the MJO flow. While the greater meridional (than zonal) gradient of the LFBS moisture field is responsible for a larger meridional moisture advection in the WIO, MC, and WP, a greater

TABLE 1. Individual term contributions associated with the PBL (1000–700 hPa) integrated MJO moisture convergence and advection for the MJO in the WIO, MC, and WP, respectively. Unit is 10^{-7} kg m^{-2} s^{-1}.

	$-(q\mathbf{\nabla}\cdot\mathbf{V})'$				$-(\mathbf{V}\cdot\mathbf{\nabla}q)'$			
	$-(\overline{q}\mathbf{\nabla}\cdot\mathbf{V}')'$	$-(q'\mathbf{\nabla}\cdot\overline{\mathbf{V}})'$	$-(q'\mathbf{\nabla}\cdot\mathbf{V}')'$	$-(q^*\mathbf{\nabla}\cdot\mathbf{V}^*)'$	$-(\overline{\mathbf{V}}\cdot\mathbf{\nabla}q')'$	$-(\mathbf{V}'\cdot\mathbf{\nabla}\overline{q})'$	$-(\mathbf{V}'\cdot\mathbf{\nabla}q')'$	$-(\mathbf{V}^*\cdot\mathbf{\nabla}q^*)'$
WIO	89.8	6.1	2.7	2.7	−6.5	27.8	−2.5	−2.2
MC	29.1	12.9	−1.1	−0.2	−1.2	13.4	5.0	0.9
WP	107.1	10.4	2.4	3.9	−6.0	8.0	−0.6	−5.4

zonal moisture advection resulting from a greater zonal moisture gradient appears in the EIO. The modeling study of M09 pointed out the role of eddy activities in the MJO meridional moisture advection at 155°E. Our observational diagnosis indicates that such an effect is longitude dependent. The synoptic eddy–induced moisture advection has a negative impact on the moisture ahead of MJO convection in the WIO, EIO, and WP.

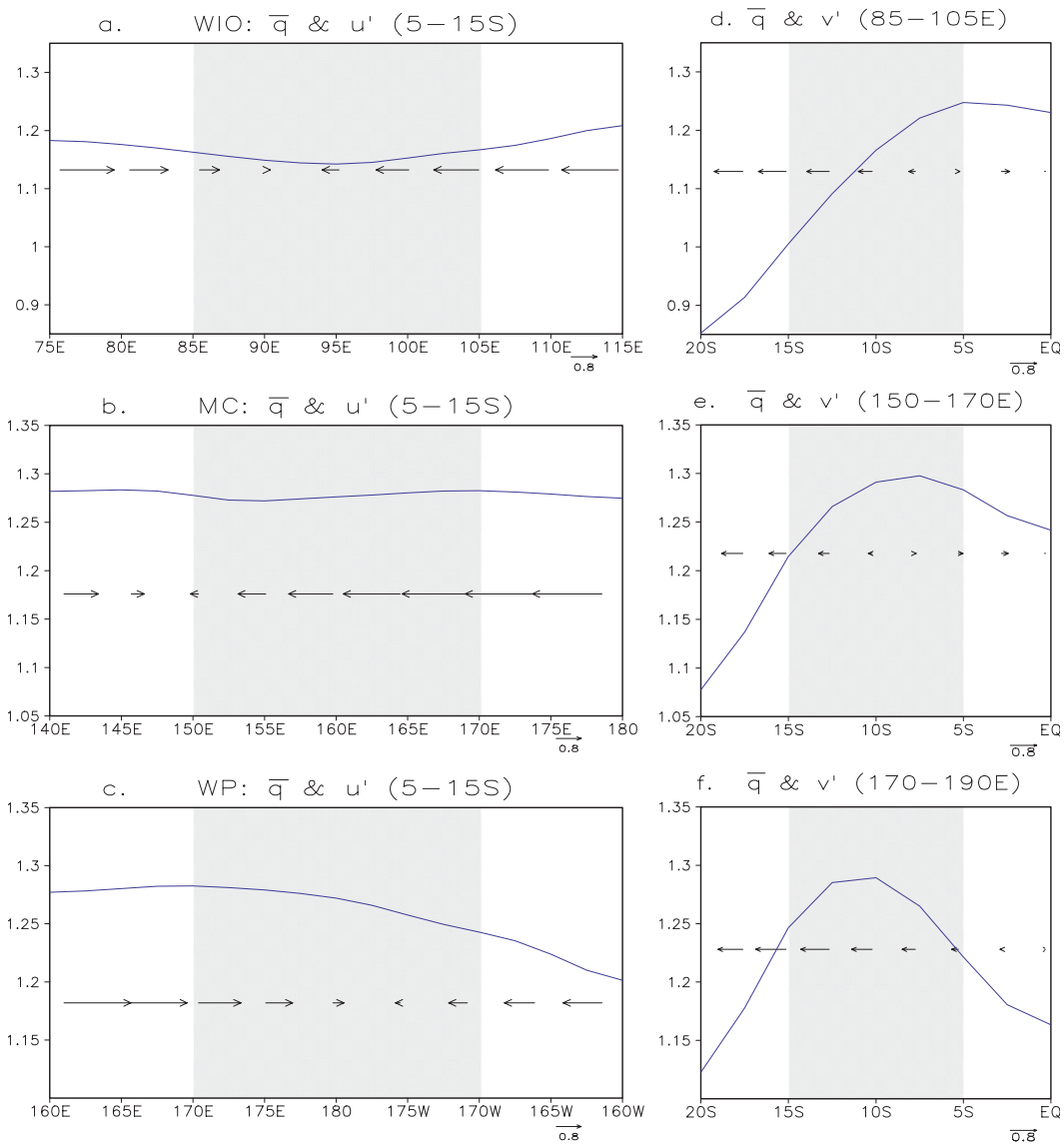

FIG. 15. As in the middle of Fig. 8, but for the MJO convection in the (top) WIO, (middle) MC, and (bottom) WP regions.

A weak positive eddy contribution was only found in the MC, and it accounts for about 5% of the total moisture advection.

It is worth mentioning that surface LHF effect is implicitly included in the apparent moisture sink term ($-Q_2/L$). To the east of MJO convection, both the enhanced precipitation due to shallow congestus and the reduced surface evaporation due to reduction in the wind speed contribute a negative moisture tendency. As a result, the apparent heating term contributes negatively to the PBL moistening ahead of convection. While the ($-Q_2/L$) term does not favor the eastward propagation, a warm SST anomaly due to the decreased local surface LHF appears to the east of the MJO convection. Previous studies suggested that the induced warm SSTA due to air–sea interaction may strengthen the MJO variance and favor the eastward propagation (Sperber et al. 1997; Waliser et al. 1999; Maloney and Sobel 2004). However, how and to what extent the warm SSTA affects the MJO remains elusive. Through a diagnosis of the PBL momentum budget in a simplified boundary layer model (Wang and Li 1993), the contribution to the PBL convergence by the SST gradient–induced pressure gradient (Lindzen and Nigam 1987) and heating-induced free-atmospheric wave dynamics is quantitatively measured. The Kelvin wave low pressure response to the MJO convection at top of the PBL accounts for 75%–90% of the total boundary layer convergence, while the SSTA gradient contributes about 10%–25% of the boundary layer convergence. The result suggests that both the internal atmospheric dynamics and air–sea interactions contribute to the PBL convergence and moisture asymmetry and thus are responsible for the eastward propagation of MJO.

A caution is needed in connecting the concept of the potential (or convective) instability and the actual occurrence of convection as there is not necessarily a causal link between the two and a large-scale layer lifting to saturation is required. The moisture budget diagnosis above may provide observational support for validating general circulation model results. In this study we focused on the lower-tropospheric moisture budget and found that the synoptic eddy contribution is in general small. Given that various recent studies emphasized the role of the synoptic eddy momentum flux and its feedback to MJO (e.g., Majda and Biello 2004; Majda and Stechmann 2009), in an accompanying paper we will address this issue based on the diagnosis of a high-resolution reanalysis dataset from ECMWF during the years of tropical convection (YOTC). In addition we will also examine the possible upscale feedback of the synoptic-scale eddy on atmospheric heating (Hsu and Li 2011) and surface heat fluxes (Zhou and Li 2010) associated with the eastward propagation of MJO in boreal winter.

Acknowledgments. Comments from anonymous reviewers are greatly appreciated. This work was supported by NSF Grant AGS-1106536, NOAA Grant NA11OAR4310087, and by the International Pacific Research Center that is sponsored by the Japan Agency for Marine-Earth Science and Technology (JAMSTEC), NASA (NNX07AG53G), and NOAA (NA17RJ1230).

REFERENCES

Araligidad, N. M., and E. D. Maloney, 2008: Wind-driven latent heat flux and the intraseasonal oscillation. *Geophys. Res. Lett.,* **35,** L04815, doi:10.1029/2007GL032746.

Benedict, J., and D. A. Randall, 2007: Observed characteristics of the MJO relative to maximum rainfall. *J. Atmos. Sci.,* **64,** 2332–2354.

Bladé, I., and D. L. Hartmann, 1993: Tropical intraseasonal oscillations in a simple nonlinear model. *J. Atmos. Sci.,* **50,** 2922–2939.

Bretherton, C. S., M. E. Peters, and L. E. Back, 2004: Relationships between water vapor path and precipitation over the tropical oceans. *J. Climate,* **17,** 1517–1528.

Brown, R. G., and C. Zhang, 1997: Variability of mid-tropospheric moisture and its effect on cloud-top height distribution during TOGA COARE. *J. Atmos. Sci.,* **54,** 2760–2774.

Chang, C.-P., and H. Lim, 1988: Kelvin-wave CISK: A possible mechanism for the 30-50-day oscillation. *J. Atmos. Sci.,* **45,** 1709–1720.

Emanuel, K. A., 1994: *Atmospheric Convection*. Oxford University Press, 580 pp.

Fu, X., B. Wang, T. Li, and J. McCreary, 2003: Coupling between northward-propagating ISO and SST in the Indian Ocean. *J. Atmos. Sci.,* **60,** 1733–1753.

Hendon, H. H., and M. L. Salby, 1994: The life cycle of Madden–Julian oscillation. *J. Atmos. Sci.,* **51,** 2207–2219.

Holloway, C. E., and J. D. Neelin, 2009: Moisture vertical structure, column water vapor, and tropical deep convection. *J. Atmos. Sci.,* **66,** 1665–1683.

Holton, J. R., 1992: *An Introduction to Dynamic Meteorology.* 3rd ed. Academic Press, 511 pp.

Houze, R. A., Jr., 1993: *Cloud Dynamics*. Academic Press, 573 pp.

Hsu, P.-C., and T. Li, 2011: Interactions between boreal summer intraseasonal oscillations and synoptic-scale disturbances over the western North Pacific. Part II: Apparent heat and moisture sources and eddy momentum transport. *J. Climate,* **24,** 942–961.

Jiang, X., and T. Li, 2005: Reinitiation of the boreal summer intraseasonal oscillation in the tropical Indian Ocean. *J. Climate,* **18,** 3777–3795.

Johnson, R. H., T. M. Rickenbach, S. A. Rutledge, P. E. Ciesielski, and W. H. Schubert, 1999: Trimodal characteristics of tropical convection. *J. Climate,* **12,** 2397–2418.

Jones, C., and B. C. Weare, 1996: The role of low-level moisture convergence and ocean latent heat fluxes in the Madden–Julian oscillation: An observational analysis using ISCCP data and ECMWF analyses. *J. Climate,* **9,** 3086–3140.

Kemball-Cook, S. R., and B. C. Weare, 2001: The onset of convection in the Madden–Julian oscillation. *J. Climate,* **14,** 780–793.

Kikuchi, K., and Y. N. Takayabu, 2004: The development of organized convection associated with the MJO during TOGA COARE IOP: Trimodal characteristics. *Geophys. Res. Lett.,* **31,** L10101, doi:10.1029/2004GL019601.

Kiladis, G. N., K. H. Straub, and P. T. Haertel, 2005: Zonal and vertical structure of the Madden–Julian oscillation. *J. Atmos. Sci.,* **62,** 2790–2809.

Kim, D., and Coauthors, 2009: Application of MJO simulation diagnostics to climate models. *J. Climate,* **22,** 6413–6436.

Lau, K.-M., and L. Peng, 1987: Origin of low-frequency (intraseasonal) oscillations in the tropical atmosphere. Part I: The basic theory. *J. Atmos. Sci.,* **44,** 950–972.

Li, T., and B. Wang, 1994: The influence of sea surface temperature on the tropical intraseasonal oscillation: A numerical study. *Mon. Wea. Rev.,* **122,** 2349–2362.

——, and C. Zhou, 2009: Planetary scale selection of the Madden–Julian oscillation. *J. Atmos. Sci.,* **66,** 2429–2443.

——, F. Tam, X. Fu, T. Zhou, and W. Zhu, 2008: Causes of the intraseasonal SST variability in the tropical Indian Ocean. *Atmos.–Ocean Sci. Lett.,* **1,** 18–23.

Liebmann, B., and C. A. Smith, 1996: Description of a complete (interpolated) outgoing longwave radiation dataset. *Bull. Amer. Meteor. Soc.,* **77,** 1275–1277.

Lin, J.-L., and Coauthors, 2006: Tropical intraseasonal variability in 14 IPCC AR4 climate models: Part I: Convective signals. *J. Climate,* **19,** 2665–2690.

Lindzen, R. S., and S. Nigam, 1987: On the role of sea surface temperature gradients in forcing low-level winds and convergence in the tropics. *J. Atmos. Sci.,* **44,** 2418–2436.

Madden, R. A., and P. R. Julian, 1971: Detection of a 40–50-day oscillation in the zonal wind in the tropical Pacific. *J. Atmos. Sci.,* **28,** 702–708.

——, and ——, 1972: Description of global-scale circulation cells in the tropics with a 40–50-day period. *J. Atmos. Sci.,* **29,** 1109–1123.

——, and ——, 2005: Historical perspective. *Intraseasonal Variability in the Atmosphere-Ocean Climate System,* K. M. Lau and D. E. Waliser, Eds., Praxis, 1–18.

Majda, A. J., and J. A. Biello, 2004: A multiscale model for tropical intraseasonal oscillations. *Proc. Natl. Acad. Sci. USA,* **101,** 4736–4741.

——, and S. N. Stechmann, 2009: A simple dynamical model with features of convective momentum transport. *J. Atmos. Sci.,* **66,** 373–392.

Maloney, E. D., 2009: The moist static energy budget of a composite tropical intraseasonal oscillation in a climate model. *J. Climate,* **22,** 711–729.

——, and D. L. Hartmann, 1998: Frictional moisture convergence in a composite life cycle of the Madden–Julian oscillation. *J. Climate,* **11,** 2387–2403.

——, and A. H. Sobel, 2004: Surface fluxes and ocean coupling in the tropical intraseasonal oscillation. *J. Climate,* **17,** 4368–4386.

Reynolds, R., N. Rayner, T. M. Smith, D. C. Stokes, and W. Wang, 2002: An improved in situ and satellite SST analysis for climate. *J. Climate,* **15,** 1609–1625.

Salby, M. L., R. Garcia, and H. H. Hendon, 1994: Planetary-scale circulations in the presence of climatological and wave-induced heating. *J. Atmos. Sci.,* **51,** 2344–2367.

Sherwood, S. C., 1999: Convective precursors and predictability in the tropical western Pacific. *Mon. Wea. Rev.,* **127,** 2977–2991.

Shinoda, T., H. H. Hendon, and J. Glick, 1998: Intraseasonal variability of surface fluxes and sea surface temperature in the tropical western Pacific and Indian Ocean. *J. Climate,* **11,** 1685–1702.

Sperber, K. R., 2003: Propagation and the vertical structure of the Madden–Julian oscillation. *Mon. Wea. Rev.,* **131,** 3018–3037.

——, J. M. Slingo, P. M. Inness, and W. K.-M. Lau, 1997: On the maintenance and initiation of the intraseasonal oscillation in the NCEP/NCAR reanalysis and in the GLA and UKMO AMIP simulations. *Climate Dyn.,* **13,** 769–795.

Takayabu, Y. N., J. Yokomori, and K. Yoneyama, 2006: A diagnostic study on interactions between atmospheric thermodynamic structure and cumulus convection over the tropical western Pacific Ocean and over the Indochina Peninsula. *J. Meteor. Soc. Japan,* **84,** 151–169.

Uppala, S. M., and Coauthors, 2005: The ERA-40 Re-Analysis. *Quart. J. Roy. Meteor. Soc.,* **131,** 2961–3012.

Waliser, D. E., 2006: Intraseasonal variations. *The Asian Monsoon,* B. Wang, Ed., Springer, 203–257.

——, K. M. Lau, and J. H. Kim, 1999: The influence of coupled sea surface temperatures on the Madden–Julian oscillation: A model perturbation experiment. *J. Atmos. Sci.,* **56,** 333–358.

Wang, B., 1988: Dynamics of tropical low frequency waves: An analysis of moist Kelvin waves. *J. Atmos. Sci.,* **45,** 2051–2065.

——, and H. Rui, 1990: Dynamics of the coupled moist Kelvin–Rossby wave on an equatorial β plane. *J. Atmos. Sci.,* **47,** 397–413.

——, and T. Li, 1993: A simple tropical atmospheric model of relevance to short-term climate variation. *J. Atmos. Sci.,* **50,** 260–284.

——, and ——, 1994: Convective interaction with boundary-layer dynamics in the development of a tropical intraseasonal system. *J. Atmos. Sci.,* **51,** 1386–1400.

Weare, B. C., P. T. Strub, and M. D. Samuel, 1981: Annual mean surface heat fluxes in the tropical Pacific Ocean. *J. Phys. Oceanogr.,* **11,** 705–717.

Wheeler, M., and G. N. Kiladis, 1999: Convectively coupled equatorial waves: Analysis of clouds and temperature in the wavenumber–frequency domain. *J. Atmos. Sci.,* **56,** 374–399.

Yanai, M., S. Esbensen, and J.-H. Chu, 1973: Determination of bulk properties of tropical cloud clusters from large-scale heat and moisture budgets. *J. Atmos. Sci.,* **30,** 611–627.

Yu, L., and R. A. Weller, 2007: Objectively analyzed air–sea heat fluxes for the global ice-free oceans (1981–2005). *Bull. Amer. Meteor. Soc.,* **88,** 527–539.

Zhang, C., 2005: The Madden–Julian oscillation. *Rev. Geophys.,* **43,** RG2003, doi:10.1029/2004RG000158.

Zhou, C., and T. Li, 2010: Upscale feedback of tropical synoptic variability to intraseasonal oscillations through the nonlinear rectification of the surface latent heat flux. *J. Climate,* **23,** 5738–5754.